

# Predicting Binding Free Energies for DPS Protein-DNA Complexes and Crystals Using Molecular Dynamics

*Eduard V. Tereshkin*<sup>1</sup> , *Ksenia B. Tereshkina*<sup>1</sup> , *Yurii F. Krupyanski*<sup>1</sup> 

© The Authors 2022. This paper is published with open access at SuperFri.org

The interaction between deoxyribonucleic acid (DNA) and deoxyribonucleic acid-binding protein from starved cells (DPS) in bacterial cells leads to intracellular crystallization of the genetic material of bacteria, which contributes to the survival of bacteria under stress factors, including antibacterial agents. Molecular modeling can help explain the molecular mechanisms of DNA binding to this protein. In this paper, we report a supercomputer simulation of the molecular dynamics of several types DNA-DPS complexes and crystals ranging from DPS+DNA dimer to DNA in periodic crystal channels of *Escherichia coli* DPS protein using a coarse-grained Martini force field. By modeling DNA of 24 base pairs, comparable in size to the diameter of the DPS protein, we use the slow-growth thermodynamic integration method to find binding protein-DNA free energy and discuss the contribution of ions and the length of trajectories sufficient for this type of simulations. The results obtained are important for further research in the field of simulation of biological DNA-protein crystals and the study of the molecular mechanisms of DNA interaction with the DPS protein.

*Keywords: molecular dynamics, slow-growth thermodynamic integration method, DPS protein, DNA stabilization, DNA-DPS binding free energy.*

## Introduction

The formation of intracellular crystals of bacterial DNA in response to stress bears much interest both in biophysics and pharmaceuticals, as well as in industry. Despite the confirmation of the formation of the crystals by DPS proteins and their homologues, the search for DNA positions in such crystals remains of immediate importance. Bacteria have numerous strategies that allow them to survive unfavorable environmental conditions [21]. The preservation of a part of the bacterial colony under stressful conditions is the key to the survival of the population in the long term [39]. Primarily, survival depends on the cell's ability to retain its DNA. Unlike eukaryotic cells, bacterial cells do not have a system of histone proteins and unified mechanisms for chromosome condensation. However, prokaryotic DNA is also capable of compacting, undergoing hierarchical packaging [41]. The chromosomal DNA of bacteria is compactly folded into the so-called nucleoid, consisting of DNA, RNA and proteins, which differs sharply from the rest of the cytoplasm. Bacteria use a number of nucleoid-associated proteins (NAPs) that influence the lower-level organization of the nucleoid by bending, stiffening, bunching, wrapping, or bridging the DNA [2, 18, 33, 41]. Bacterial chromatin can change its shape and composition depending on the growth phase of bacterial population and the state of the cells. During prolonged starvation, DNA, together with bacterial NAPs, can form various condensed structures [17, 23]. One of the most notable strategies is the crystallization of the bacterial nucleoid with the help of DPS proteins (DNA-binding Proteins from Starved cells) and their homologues [42]. DPS was first isolated from cells of *Escherichia coli* (*E. coli*) under stress of starvation [1]. Studies of bacteria and archaea revealed a wide distribution of proteins of the DPS family and proteins homologous to them among the representatives of these domains. The crystal structure of *E. coli* DPS was first obtained in 1998 by X-ray diffraction analysis with a resolution of 1.6 Å [9]. DPS forms a

<sup>1</sup>N. N. Semenov Federal Research Center for Chemical Physics, Russian Academy of Sciences, Moscow, Russian Federation

dodecamer with 23 (tetrahedral) point group symmetry. It has a spherical shape with a cavity inside ( $\sim 9$  nm outer diameter,  $\sim 5$  nm inner diameter) and pores at the three-folds.

During the logarithmic phase of growth, DPS has been shown to be a minor component of the nucleoid ( $\sim 6$  thousand molecules per cell). In the stationary phase, its synthesis sharply increases, and DPS becomes the predominant nucleoid-associated protein ( $\sim 180$  thousand molecules per cell [14]. DPS can protect bacteria against multiple stresses during stationary phase of grow [27]. The conventional point of view that DPS binds DNA without sequence or structural specificity, but there is controversial data [3]. The structure of this protein and probable interactions with DNA was studied *in vitro* [6, 7, 9, 16, 26, 34]. *In silico* studies have shown how the DPS protein can form crystals and co-crystals with DNA under various conditions [36–38]. The long N-terminal regions and the surface of the protein are rich in lysine residues. Like the tails of eukaryotic histone proteins [12, 32], the N-terminals of DPS provide stability and conformational mobility of DNA, and also determine the binding of DNA to DPS protein complexes. However, the amino acid sequences and structures of bacterial NAPs and eukaryotic histones differ greatly. The spherical shape of the molecule allows the formation of crystals with different unit cell parameters and space groups, all of which have extended channels inside.

Presumably, during *in vivo* crystallization, DNA can be located inside the channels of DPS crystals and on the surface of DPS molecules. Unfortunately, it has not yet been possible to resolve the structure of DPS crystals in which the DNA coordinates would be obtained and the location of the DNA would be shown. Therefore, in this work, using computer simulation, we tried to obtain putative molecular structures of DPS clusters and crystals with DNA and make an attempt to evaluate the advantageous position of DNA in one or another of them. The aim of this work was to find favorable DNA positions relative to the DPS protein using molecular dynamics modeling by suitable protocols.

## 1. Methods

### 1.1. Building of the Molecular Models

Each subunit of *E. coli* DPS protein contains 167 amino acid residues. It consists of four long  $\alpha$ -helices parallel to each other and one small  $\alpha$ -helix perpendicular to them [5]. The N-terminal regions of the molecule consist of ordered and disordered parts. The ordered part of each N-terminus (amino acid residues numbered 14 till 25) can be easily deciphered by X-ray diffraction analysis [9, 15]. The three-dimensional structure of the disordered part of the N-terminus is not defined in any structure of the RCSB Protein Data Bank. As shown in our work [38], this is due to the extreme mobility of these regions of the molecule. N-termini and C-termini provide connection of DPS monomers in dodecamers, binding of dodecamers between themselves and with DNA. We have modelled a spatial structure of the DPS protein and its 2D and 3D crystals on the basis of the crystal structure 6GCM.pdb. Because the file lacks the positions of the flexible amino acid residues from the unordered part of all the N-termini, we added them using UCSF Chimera program package [30]. Each N-terminus was modeled separately rather than copying the same spatial structure for all 12 fragments [38].

Double-stranded linear DNA fragments, containing 24 base pairs, 5'-AAGTCGACCCTAGAGGATCTTTGT-3', were used to build the DNA-DPS complexes. Three-dimensional models of DPS crystals, DNA-DPS clusters and co-crystals were constructed

in the UCSF Chimera program package. The systems were placed in a periodic box. We modeled systems both with counterions only and with ions at concentrations corresponding to physiological concentrations in the *E. coli* cells [35]. It should be noted that the set of “ions” in the MARTINI force field is poor and consist not of usual ions, but of charged particles that imitate hydrated ions. Therefore, here we are only talking about concentrations, not about the exact ionic composition. Ion names are given according to *martini.v2.0.ions.itp* topology file. Counterions, namely 48 sodium ions per protein molecule and 46 sodium ions per one DNA molecule were added to the systems to maintain their electrical neutrality. Then the rest of the ions were added to the same system to obtain the ion concentration of *E. coli* cells. Since DPS crystals are large, the systems were studied in the coarse-grained approximation. Models were built and verified using the MARTINI 2.1\_DNA coarse-grained force field [20, 40]. We used *dssp* program for protein structure assignment. The Python scripts *martinize.py* [13] and *martinize-dna.py* were used to convert atomistic protein and DNA molecules, respectively, to MARTINI coarse grain structures and topologies. The topology files contained standard constraints used in the MARTINI force field to maintain the secondary structure elements such as  $\alpha$ -helices of protein. Elastic Network in Dynamics (elnedyn22 modification) was used for DNA [29, 40].

Due to the use of large particles when describing water molecules (one “molecule” of water in MARTINI corresponds to four all-atom water molecules), in the MARTINI force field, even with correctly selected molecular dynamics protocols, artifact freezing of water in the system is possible [10]. Depending on the simulation conditions, in the temperature range of 280K–300K [19], nucleation and freezing of the entire volume of water in the simulation box are observed. For our systems, we observed this process at 300K. To avoid this, we replaced at least 10% of the non-polarizable water beads (W) by anti-freeze [19] water beads (WF). The difference between “antifreeze” water and “ordinary” water is as follows. Non-bonded interactions of MARTINI particles are described by shifted Lennard-Jones 12-6 potential energy function (1)

$$U_{LJ}(r) = 4\epsilon_{ij} \left[ \left( \frac{\sigma_{ij}}{r} \right)^{12} - \left( \frac{\sigma_{ij}}{r} \right)^6 \right], \quad (1)$$

where  $\sigma_{ij}$  represents the closest distance of approach between two particles  $i$  and  $j$ ,  $\epsilon_{ij}$  is the strength of their interaction. For most interacting pairs, including pairs with ordinary water beads,  $\sigma_{ij} = 0.47$  nm. For water and antifreeze water interactions,  $\sigma_{W-WF} = 0.57$  nm, that makes it possible to disturb the lattice packing of the uniformly sized solvent particles. To avoid phase separating of antifreeze and other water particles,  $\epsilon_{W-WF} = 5.6$  kJ/mol vs  $\epsilon_{W-W} = \epsilon_{WF-WF} = 5.0$  kJ/mol. Antifreeze water beads are not distinguishable for particles of other types, because of the same values of  $\sigma$  and  $\epsilon$  as for ordinary water.

6GCM crystals contain an extensive network of channels. Three types of mutually orthogonal channels were found inside the crystal, surrounded (if we consider the cut in a plane perpendicular to the channel) by four DPS molecules: fairly wide channels of the first type (denoted as x) and narrow channels of the second (y) and the third types (z). Also in the crystal there are short channels surrounded by three DPS molecules (denoted as 3). It is assumed that the DNA in the channels is arranged randomly, filling the channels with bends from one channel to another. In this work, we studied a crystal in which short DNA fragments are packed into channels of all four types. DNA bends were not considered.

We examined both DNA in periodic crystal channels and DPS clusters. Clusters were obtained by cutting out 3 or 4 DPS molecules from the crystal, surrounding a channel. Table 1 informs on the composition of the various DNA and DNA-DPS systems. The DPS dodecamer contains 4344 coarse-grained particles, the double-stranded DNA molecule (24 base pairs) is built from 310 particles.

**Table 1.** The number of coarse-grained particles in simulated systems. In the *Name* column, 2D are two-dimensional periodic crystals, 3D are three-dimensional periodic crystals. Designations in brackets: 3, x, y, z are the names of the channels (see in the text), c/i – only counterions are added to the system. The number of molecules for DNA and DPS, and the number of coarse-grained particles for ions and water are shown. W – water, WF – antifreeze water

Name	DPS	DNA	NA <sup>+</sup>	CL <sup>-</sup>	CA <sup>2+</sup>	W	WF
DNA	-	1	46	-	-	13212	1468
DNA (c/i)	-	1	252	208	1	12838	1427
1DPS	1	1	816	740	4	34942	3882
1DPS (c/i)	1	1	94	-	-	36252	4028
2DPS (c/i)	2	1	142	-	-	94860	10540
3DPS (c/i)	3	1	190	-	-	97920	10880
4DPS (x)	4	1	2750	2544	16	124046	13782
4DPS (x, c/i)	4	1	238	-	-	128610	14290
4DPS (y, c/i)	4	1	238	-	-	115380	12820
2D	4	1	814	584	4	34352	3817
3D (3)	8	1	599	175	3	19227	2136
3D (x)	8	1	599	175	3	19240	2134
3D (x, c/i)	8	1	430	-	-	19517	2168
3D (y)	8	1	599	175	3	19282	2142
3D (z)	8	1	599	175	3	19280	2138

## 1.2. Molecular Dynamics Simulations

Molecular modeling of every system included two stages: classical dynamics simulation and the search for free energy by the slow-growth thermodynamics integration (TI) method. The first stage was to obtain stable DNA conformations at the protein surface and in solution. We followed our earlier established simulation protocols. Energy minimization using steepest descent algorithm followed by relaxation at constant volume (100 ps) and constant pressure (100 ps). Then we ran simulations in the NPT ensemble at 300 K and 1 bar controlled by means of a velocity Langevin thermostat [8] with a time constant of 1 ps and a Parrinello-Rahman barostat [28] with a time constant of 4 ps, respectively. The barostat provided isotropic pressure coupling for all systems, with the exception of two-dimensional periodic crystals, for which the pressure regulation was semi-isotropic. The isothermal compressibility of water was  $4.5 * 10^{-5} \text{ bar}^{-1}$ . The fastest degrees of freedom were removed by the parallel linear constraint solver. A cutoff radii of 1.2 nm was used for Coulombic and van der Waals interactions. The

integration step was 10 fs, providing trajectories up to 100000000 steps. The dielectric constant of the medium was equal to 15 for implicit screening. The simulations were carried out with the Gromacs 5.1 package [11].

Then we performed free energy simulations using TI. We were interested in the free energy differences between DNA in DNA-DPS clusters and crystals and DNA in solution (2). The binding free energy,  $\Delta G = -\Delta G_1$ , is a work required to transfer a DNA molecule from the solution (water+ions) into protein-DNA complex and was calculated according the thermodynamic cycle shown in Fig. 1. This cycle can be expanded by other contributions [24, 25]. In Fig. 1 DNA (24 base pairs) is shown in red. The DPS molecule is shown in blue; instead of a single DPS molecule, we also considered DPS clusters and crystals. In Fig. 1,  $\Delta G = -\Delta G_2$  is the work required to remove all the internal nonbonded (Coulombic and van der Waals) interactions of DNA in DPS cluster or crystal with surroundings. This was achieved by the gradual transformation of DNA atoms from fully interacting with the environment to completely non-interacting, which DNA state is designated in the figure as “DNA ghost”. Non-interacting atoms do not keep unbonded interactions, but completely keep their masses and intramolecular bonded interactions. In this case, we used a series of TI simulations. The work required to transfer the completely non-interacting DNA from DNA-protein complex to solution,  $\Delta G = -\Delta G_3$ . The term is effectively zero due to volume equality and lack of interaction with the surroundings.  $\Delta G = -\Delta G_4$  is the work required to turn DNA into a non-interacting “ghost” DNA in solution. To obtain it, we also used a series of TI simulations.

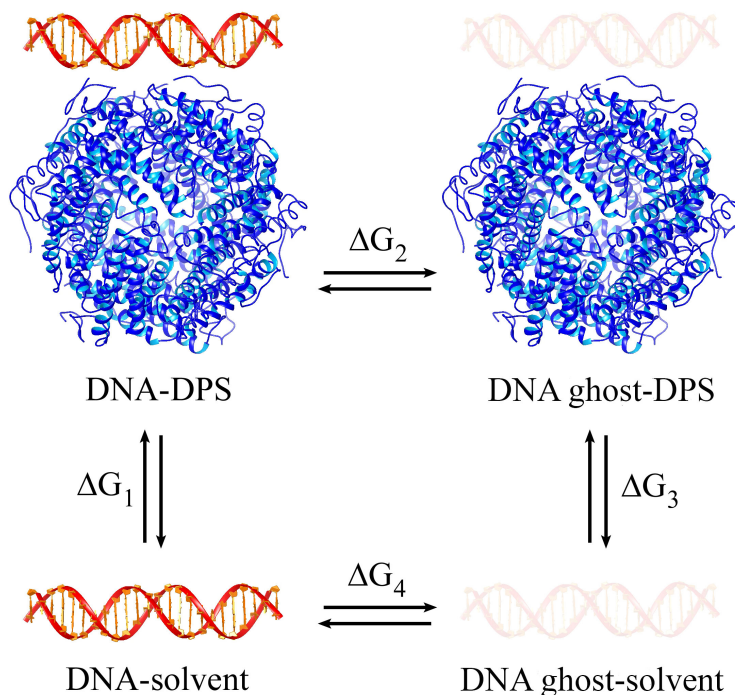


**Figure 1.** Thermodynamic cycle for the determination of binding free energies for DNA-DPS cluster. DPS protein is shown in blue, DNA is red. “DNA ghost” is the DNA that is completely non-interacting with surroundings

$$\Delta\Delta G = \Delta G_1 = \Delta G_4 - \Delta G_3 - \Delta G_2 \quad (2)$$

We chose the slow-growth thermodynamic integration method because it allows us to obtain DNA binding energies inside DPS crystals without destroying them. It is known that the Hamiltonian of the system in the slow-growth method becomes dependent on the coupling parameter,  $\lambda$ :  $H=H(p,q;\lambda)$ , where  $p$  and  $q$  are momenta and coordinates of the particles, respectively. In our simulations, Coulomb and Lennard-Jones terms were controlled by  $\lambda$  independently. The number of coupling parameter values varied to achieve computational efficiency. This will be described in more detail below. To ensure convergence when particles grow out of nothing, the regular Lennard-Jones and Coulomb potentials were modified with soft-core potentials [31]. The soft-core parameter was 0.5, the soft-core  $\lambda$  power was 1, the power of the radial term in the soft-core equation was 6 as recommended for the MARTINI force field. For each value of the coupling parameter, energy minimization and equilibrations were performed according to the protocol described above. The production run was simulated up to 30 ns. The frequency for writing  $dH/d\lambda$  was 0.1 ps. Bennetts Acceptance Ratio (BAR) method [4] was used for calculating values of  $\Delta G$  for transformations from two states using the *bar* module of Gromacs.

## 2. Results and Discussion

### 2.1. Free DNA and 1DPS-DNA Clusters

The systems of DNA in solution and DNA bound to single DPS molecule were considered to develop a protocol for calculating the Gibbs free energy. Using the coupling parameter, we gradually increased from zero the van der Waals interactions between DNA and the environment at the electrostatic interactions turned off. When the van der Waals interactions became fully turned on, we gradually increased the electrostatic interactions. This correspond to  $\Delta G = -\Delta G_4$  and  $\Delta G = -\Delta G_2$  calculation. Unless otherwise noted, simulations were made for of DNA configuration in solution at 30 ns and DNA with protein at 0.2  $\mu$ s of the classical trajectory.

In Fig. 2a one can see the  $\Delta G = -\Delta G_4/N$  depending on the simulation time of the TI trajectory.  $N = 24$  is the number of base pairs of DNA. For computational efficiency, we tried to find the minimum number of well-chosen values of the coupling parameter  $N(\lambda)$  by testing between 42 and 200  $\lambda$  values, and trajectory lengths sufficient to estimate the energies. We recalculated the values of the Gibbs energy every 1 ns starting from the trajectory time of 2 ns to track the output of the function to a plateau, the points are shown in the figure by triangles (DNA-solution) or circles (DNA-DPS). Curves with pink triangles (circles) correspond to simulations with counterions, with blue triangles to simulations with the *E. coli* cell concentration of ions (*E. coli* ions) [35].

DNA in solution and a DNA cluster with one DPS molecule with counterions was considered as the simplest model. Choosing  $\Delta\lambda=0.01$ , we simulated 200 trajectories with different values of  $\lambda$  (blue curve in Fig. 2a). Reducing  $N(\lambda)$  to 42 made it possible to increase the simulation performance by a factor of 5, while a change in the free energy value of only 1.5% was observed (brown curve in Fig. 2a). This value  $-2.2$  kJ/mol is less than the statistical error ( $\pm 3.1$  kJ/mol). It provides sufficient overlap of the phase space. A further decrease in  $N(\lambda)$  is impractical, as it leads to results that violate the second law of thermodynamics because of undersampling regardless of the length of the trajectory. Unfortunately, it is difficult to judge the quality of the obtained data due to the impossibility of obtaining the values of the free energy of solvation of this DNA by experimental methods. However, the obtained values are in good agreement with other data on the solvation of nucleic bases [22].

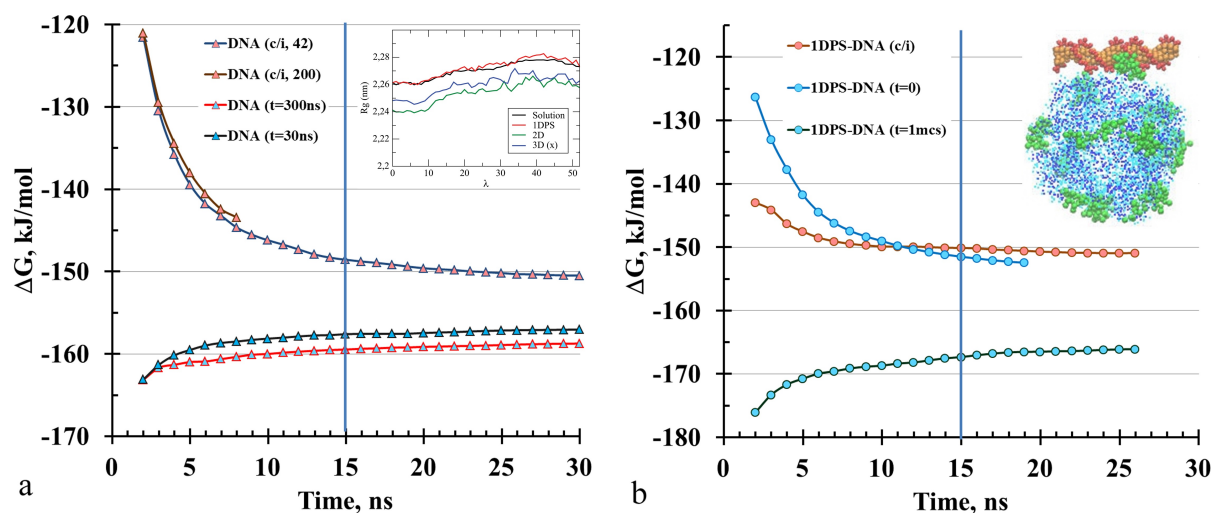


**Figure 2.** The change in the Gibbs energy for the transition of DNA from completely non-interacting to fully interacting with the solution (a) and with one DPS molecule in the solution (b). The insets show DNA radius of gyration (a) in different systems and the structure of a DNA cluster with one DPS molecule (b). DNA molecule is shown in red, DPS molecule is blue, mobile N-termini of DPS (1-20 terminal residues) are green

Simulations of DNA at *E. coli* ion concentration in solution and with DPS were chosen to demonstrate how the time of the original classical trajectory may affect free energy calculations. As starting points for TI, the conformations of the system were taken at two points of the classical trajectory, namely 30 ns (Fig. 2a black line) and 300 ns (Fig. 2a red line). The difference in free energy values turned out to be about 5% ( $-8.25$  kJ/mol). As it can be seen from the comparison of the blue and red curves, a solution with *E. coli* ions seems to be more energetically favorable for DNA than a solution with counterions. Inset in Fig. 2a shows that the radius of DNA gyration practically does not change from  $\lambda$ , regardless of the considered system (free DNA or DNA-protein).

Figure 2b shows that the value of the Gibbs energy ( $-\Delta G_2$ ) of a DNA cluster with one DPS molecule (see the structure in the inset) is affected by both the ionic composition and the adjustment of the ionic and protein environment. A change in the conformation of the protein may also be important, but verification of this was beyond the scope of this work. The starting point of preliminary dynamics simulation of DNA-DPS with *E. coli* ions is clearly insufficient to obtain acceptable value of the free energy, because the ionic environment does not have time to accurately rearrange (blue curve in Fig. 2b). The simulation with counterions after 100 ns dynamics (brown curve) gives a similar value. While the preliminary simulation of the system with *E. coli* ions for 1  $\mu$ s (black curve) brings lower values of the Gibbs energy. Thus, to obtain Gibbs energies, it is desirable to carry out a preliminary simulation of the dynamics of DNA in solution for at least 30 ns. As for DNA-protein complexes, a preliminary simulation of at least 100 ns is required. What about TI, it is desirable to simulate trajectories of at least 15 ns with  $N(\lambda)$  about 40 for DNA in solution and closer to 30 ns with  $N(\lambda)$  about 50 for DNA in DNA-DPS complexes.

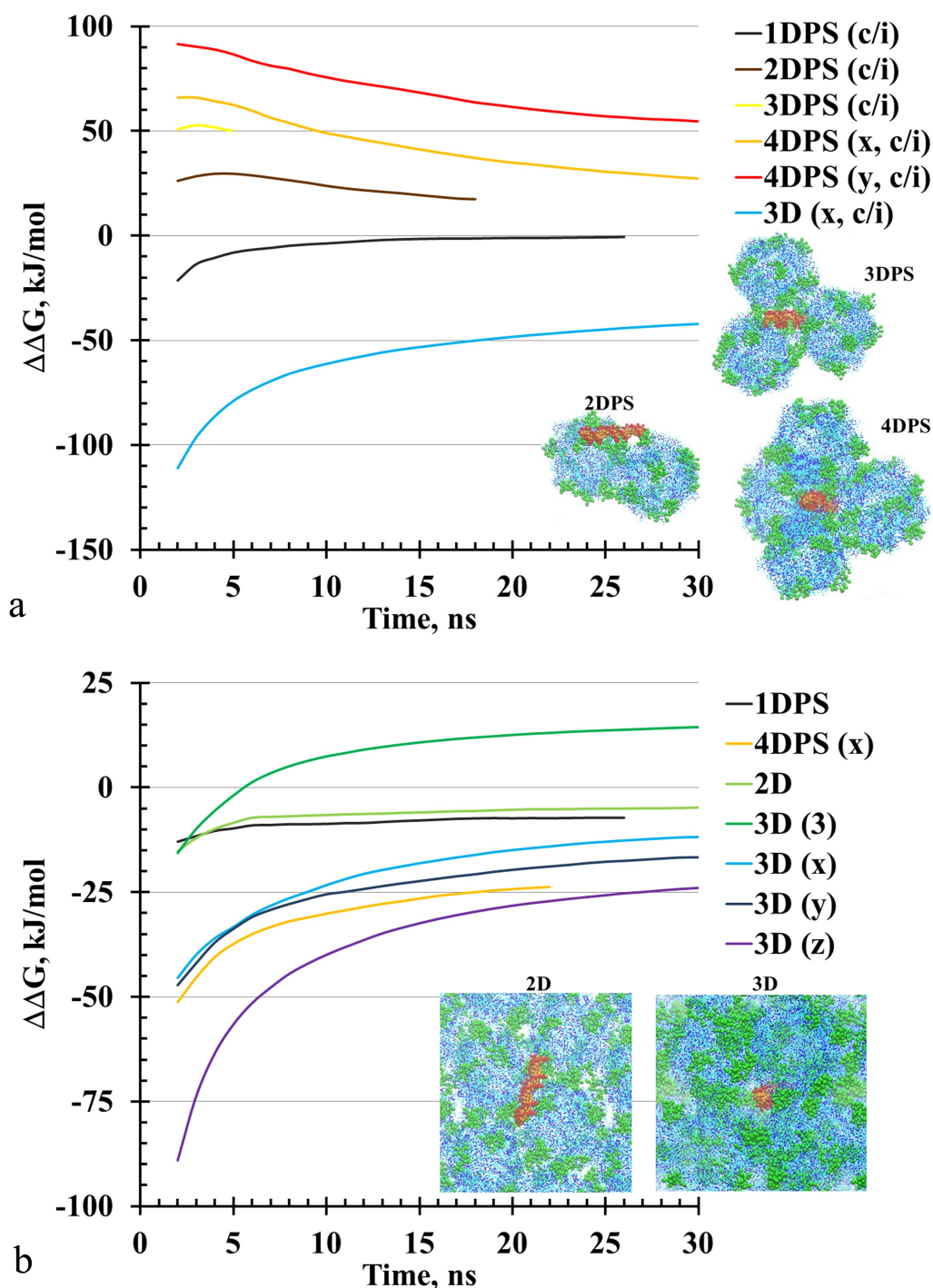
## 2.2. DNA-DPS Clusters and Crystals

Figure 3 shows the difference in Gibbs free energies according to equation (1), i.e. free energies of DNA-protein binding depending on the simulation time of TI. Average values per one base pair of DNA are given. Figure 3a shows curves for the systems with counterions, while Fig. 3b is for the *E. coli* ions. The structure of the DNA cluster with 1DPS is shown above in inset of Fig. 2b. The structure of DNA clusters with 2DPS, 3DPS, and 4DPS can be seen in Fig. 3a. Clusters of DNA-4DPS have three different shapes (denoted x, y, z) due to different positions of DPS molecules relative to each other. This is described in details in 1.1. DNA adsorbed on 2D-crystal of DPS and embedded in 3D-crystal are shown in Fig. 3b. In a crystal, DNA can be located in several directions, which corresponds to clusters with 3 DPS and 4 DPS, which is also detailed in 1.1. The composition of the systems is given in Tab. 1.

In Fig. 3a, the black curve corresponds to the free energy of DNA binding to one DPS molecule and becomes close to zero already after 15 ns of simulation and approaches the value  $\Delta\Delta G = -0.63 \pm 2.12$  kJ/mol in 26 ns. When clusters are enlarged (by adding DPS molecules), we obtain even positive values of  $\Delta\Delta G$  up to  $\sim 50$  kJ/mol per base pair, i.e., such a process is energetically unfavorable (brown, yellow, orange and red curves in Fig. 3a). However, as it can be seen from the blue curve, the presence of DNA inside the DPS crystal is favorable with  $\Delta\Delta G = -44.12 \pm 6.07$  kJ/mol. As it was shown in [38], DNA stabilizes DPS crystals due to the formation of additional interactions in the system (N-terminus of one DPS molecule)-DNA-(another DPS molecule). The black curve in Fig. 3b (DNA cluster with 1DPS) lies in the negative region. That is, in the presence of ions, the formation of such a cluster becomes advantageous with  $\Delta\Delta G = -7.21 \pm 1.32$  kJ/mol. Slightly less favorable is the adsorption of DNA on a 2D-crystals of DPS (light green curve in Fig. 3b),  $\Delta\Delta G = -4.77 \pm 1.36$  kJ/mol. It should be noted that during the formation of a cluster with one DPS molecule, only one N-terminus is involved in DNA binding. While DNA adsorption on the crystal surface, several N-termini are involved (green DPS regions in the insets). Channels bordered by three DPS molecules (green curve in Fig. 3b), as well as clusters of three DPS molecules, are unfavorable for DNA ( $\Delta\Delta G$  15kJ/mol). Presumably, these channels cannot serve as the main “warehouses” of DNA, but possibly can serve for DNA as transition regions of crystals between other channels. The presence of ions favors the growth of clusters (orange line in Fig. 3b). Binding free energy of DNA with 4 molecules of DPS is  $\Delta\Delta G = -23.76 \pm 4.39$  kJ/mol. The binding free energies of DNA in the main (blue line in Fig. 3b) and additional (blue and purple lines) channels of DPS 6GCM protein crystals are negative and equal, respectively,  $\Delta\Delta G = -11.82 \pm 5.2$  kJ/mol,  $-16.7 \pm 4.29$  kJ/mol, and  $-23.96 \pm 4.63$  kJ/mol. Nevertheless, these values are lower by absolute value than for DNA in the presence of counterions given above. Thus, the formation of DNA-DPS clusters is more favorable and possible in the presence of ions, while the retention of DNA in a bound state is more favorable at low ionic strength.

## Conclusions

In this work, we have studied the binding free energies of DNA with the DPS protein in different clusters and channels of 6PCM.pdb crystals of *Escherichia coli* DPS protein. In order to obtain acceptable values of free energy when simulating in GROMACS 5.1 with the MARTINI force field, two-stage simulations were carried out. At the first stage, we simulated the dynamics on trajectories up to  $0.2 \mu\text{s}$  (up to  $1 \mu\text{s}$  for a DNA cluster with one DPS molecule). It was



**Figure 3.** Binding Gibbs free energies of DNA (per base pair) in DNA-DPS complexes and crystals for simulation with counterions (a) and normal concentration of ions in *E. coli* cells (b). The insets show the structure of DNA-DPS clusters and crystals. DNA molecules are shown in red, DPS molecules are blue, mobile N-termini are green

shown, that the trajectories for simulation of DNA dynamics  $\sim 30$  ns are quite enough, while for DNA-DPS complexes should be not less than  $0.1 \mu\text{s}$  and longer depending on the system. Even for already formed DNA-DPS complexes, it is important to wait for the complete adjustment of the ionic environment, which requires rather long trajectories for such systems. Subsequent simulations by slow-growth thermodynamic integration method can be performed for DNA at

~40 points of the binding parameter. For computer-efficient calculation of the free energies of binding of DNA in DNA-DPS complexes (clusters and crystals), it seems optimal to choose ~50 points of the binding parameter. It has been shown that a solution with an ion concentration corresponding to that in the *E. coli* cells may be more favorable for DNA binding into DNA-protein clusters, while a solution with low ionic strength may be more optimal for co-crystals.

## Acknowledgements

The computations were carried out on MVS-10P at Joint Supercomputer Center of the Russian Academy of Sciences (JSCC RAS). This work was supported within frameworks of the state task for N. N. Semenov Federal Research Center for Chemical Physics RAS FFZE-2022-0011 (State Registration No. 122040400089-6).

*This paper is distributed under the terms of the Creative Commons Attribution-Non Commercial 3.0 License which permits non-commercial use, reproduction and distribution of the work without further permission provided the original work is properly cited.*

## References

1. Almiron, M., Link, A.J., Furlong, D., Kolter, R.: A novel DNA-binding protein with regulatory and protective roles in starved escherichia coli. *Genes & Development* 6(12b), 2646–2654 (dec 1992). <https://doi.org/10.1101/gad.6.12b.2646>
2. Amemiya, H.M., Schroeder, J., Freddolino, P.L.: Nucleoid-associated proteins shape chromatin structure and transcriptional regulation across the bacterial kingdom. *Transcription* 12(4), 182–218 (aug 2021). <https://doi.org/10.1080/21541264.2021.1973865>
3. Antipov, S.S., Tutukina, M.N., Preobrazhenskaya, E.V., *et al.*: The nucleoid protein Dps binds genomic DNA of Escherichia coli in a non-random manner. *PLOS ONE* 12(8), e0182800 (aug 2017). <https://doi.org/10.1371/journal.pone.0182800>
4. Bennett, C.H.: Efficient estimation of free energy differences from Monte Carlo data. *Journal of Computational Physics* 22(2), 245–268 (oct 1976). [https://doi.org/10.1016/0021-9991\(76\)90078-4](https://doi.org/10.1016/0021-9991(76)90078-4)
5. Chiancone, E., Ceci, P.: The multifaceted capacity of dps proteins to combat bacterial stress conditions: Detoxification of iron and hydrogen peroxide and DNA binding. *Biochimica et Biophysica Acta (BBA) - General Subjects* 1800(8), 798–805 (aug 2010). <https://doi.org/10.1016/j.bbagen.2010.01.013>
6. Dadinova, L.A., Chesnokov, Y.M., Kamyshinsky, R.A., *et al.*: Protective Dps-DNA co-crystallization in stressed cells: an in vitro structural study by small-angle X-ray scattering and cryo-electron tomography. *FEBS Letters* 593(12), 1360–1371 (2019). <https://doi.org/10.1002/1873-3468.13439>
7. Frenkiel-Krispin, D., Minsky, A.: Nucleoid organization and the maintenance of DNA integrity in *E. coli*, *B. subtilis* and *D. radiodurans*. *Journal of Structural Biology* 156(2), 311–319 (nov 2006). <https://doi.org/10.1016/j.jsb.2006.05.014>

8. Goga, N., Rzepiela, A.J., de Vries, A.H., *et al.*: Efficient algorithms for langevin and DPD dynamics. *Journal of Chemical Theory and Computation* 8(10), 3637–3649 (jun 2012). <https://doi.org/10.1021/ct3000876>
9. Grant, R.A., Filman, D.J., Finkel, S.E., *et al.*: The crystal structure of Dps, a ferritin homolog that binds and protects DNA. *Nature Structural Biology* 5(4), 294–303 (apr 1998). <https://doi.org/10.1038/nsb0498-294>
10. Hadley, K.R., McCabe, C.: Coarse-grained molecular models of water: a review. *Molecular Simulation* 38(8-9), 671–681 (jul 2012). <https://doi.org/10.1080/08927022.2012.671942>
11. Hess, B., Kutzner, C., van der Spoel, D., Lindahl, E.: GROMACS 4: algorithms for highly efficient, load-balanced, and scalable molecular simulation. *Journal of Chemical Theory and Computation* 4(3), 435–447 (feb 2008). <https://doi.org/10.1021/ct700301q>
12. Huertas, J., Cojocaru, V.: Breaths, twists, and turns of atomistic nucleosomes. *Journal of Molecular Biology* 433(6), 166744 (mar 2021). <https://doi.org/10.1016/j.jmb.2020.166744>
13. de Jong, D.H., Singh, G., Bennett, W.F.D., *et al.*: Improved Parameters for the Martini Coarse-Grained Protein Force Field. *Journal of chemical theory and computation* 9(1), 687–697 (2013). <https://doi.org/10.1021/ct300646g>
14. Karas, V.O., Westerlaken, I., Meyer, A.S.: The DNA-binding protein from starved cells (dps) utilizes dual functions to defend cells against multiple stresses. *Journal of Bacteriology* 197(19), 3206–3215 (oct 2015). <https://doi.org/10.1128/jb.00475-15>
15. Kovalenko, V., Popov, A., Santoni, G., *et al.*: Multi-crystal data collection using synchrotron radiation as exemplified with low-symmetry crystals of Dps. *Acta Crystallographica Section F Structural Biology Communications* 76(11), 568–576 (oct 2020). <https://doi.org/10.1107/s2053230x20012571>
16. Krupyanski, Y.F., Loiko, N.G., Sinityn, D.O., *et al.*: Biocrystallization in bacterial and fungal cells and spores. *Crystallography Reports* 63(4), 594–599 (jul 2018). <https://doi.org/10.1134/s1063774518040144>
17. Loiko, N., Danilova, Y., Moiseenko, A., *et al.*: Morphological peculiarities of the DNA-protein complexes in starved Escherichia coli cells. *PLOS ONE* 15(10), e0231562 (oct 2020). <https://doi.org/10.1371/journal.pone.0231562>
18. Luijsterburg, M.S., White, M.F., van Driel, R., Dame, R.T.: The major architects of chromatin: Architectural proteins in bacteria, archaea and eukaryotes. *Critical Reviews in Biochemistry and Molecular Biology* 43(6), 393–418 (jan 2008). <https://doi.org/10.1080/10409230802528488>
19. Marrink, S.J., Risselada, H.J., Yefimov, S., *et al.*: The MARTINI force field: coarse grained model for biomolecular simulations. *The Journal of Physical Chemistry B* 111(27), 7812–7824 (2007). <https://doi.org/10.1021/jp071097f>

20. Marrink, S.J., Tieleman, D.P.: Perspective on the Martini model. *Chemical Society Reviews* 42(16), 6801 (2013). <https://doi.org/10.1039/c3cs60093a>
21. Martinez, J.L.: The role of natural environments in the evolution of resistance traits in pathogenic bacteria. *Proceedings of the Royal Society B: Biological Sciences* 276(1667), 2521–2530 (apr 2009). <https://doi.org/10.1098/rspb.2009.0320>
22. Miller, J.L., Kollman, P.A.: Solvation free energies of the nucleic acid bases. *The Journal of Physical Chemistry* 100(20), 8587–8594 (jan 1996). <https://doi.org/10.1021/jp9605358>
23. Minsky, A., Shimoni, E., Frenkiel-Krispin, D.: Stress, order and survival. *Nature Reviews Molecular Cell Biology* 3(1), 50–60 (jan 2002). <https://doi.org/10.1038/nrm700>
24. Mobley, D.L., Chodera, J.D., Dill, K.A.: On the use of orientational restraints and symmetry corrections in alchemical free energy calculations. *The Journal of Chemical Physics* 125(8), 084902 (aug 2006). <https://doi.org/10.1063/1.2221683>
25. Mobley, D.L., Chodera, J.D., Dill, K.A.: Confine-and-release method: Obtaining correct binding free energies in the presence of protein conformational change. *Journal of Chemical Theory and Computation* 3(4), 1231–1235 (may 2007). <https://doi.org/10.1021/ct700032n>
26. Moiseenko, A., Loiko, N., Tereshkina, K., *et al.*: Projection structures reveal the position of the DNA within DNA-Dps Co-crystals. *Biochemical and Biophysical Research Communications* 517(3), 463–469 (sep 2019). <https://doi.org/10.1016/j.bbrc.2019.07.103>
27. Nair, S., Finkel, S.E.: Dps protects cells against multiple stresses during stationary phase. *Journal of Bacteriology* 186(13), 4192–4198 (jul 2004). <https://doi.org/10.1128/jb.186.13.4192-4198.2004>
28. Parrinello, M., Rahman, A.: Polymorphic transitions in single crystals: A new molecular dynamics method. *Journal of Applied Physics* 52(12), 7182–7190 (dec 1981). <https://doi.org/10.1063/1.328693>
29. Periole, X., Cavalli, M., Marrink, S.J., Ceruso, M.A.: Combining an elastic network with a coarse-grained molecular force field: Structure, dynamics, and intermolecular recognition. *Journal of chemical theory and computation* 5(9), 2531–2543 (2013). <https://doi.org/10.1021/ct300646g>
30. Pettersen, E.F., Goddard, T.D., Huang, C.C., *et al.*: UCSF Chimera—A visualization system for exploratory research and analysis. *Journal of Computational Chemistry* 25(13), 1605–1612 (2004). <https://doi.org/10.1002/jcc.20084>
31. Pham, T.T., Shirts, M.R.: Optimal pairwise and non-pairwise alchemical pathways for free energy calculations of molecular transformation in solution phase. *The Journal of Chemical Physics* 136(12), 124120 (mar 2012). <https://doi.org/10.1063/1.3697833>
32. Shaytan, A.K., Armeev, G.A., Goncarencu, A., *et al.*: Coupling between histone conformations and DNA geometry in nucleosomes on a microsecond timescale: Atomistic insights into nucleosome functions. *Journal of Molecular Biology* 428(1), 221–237 (jan 2016). <https://doi.org/10.1016/j.jmb.2015.12.004>

33. Shen, B.A., Landick, R.: Transcription of bacterial chromatin. *Journal of Molecular Biology* 431(20), 4040–4066 (sep 2019). <https://doi.org/10.1016/j.jmb.2019.05.041>
34. Sinitsyn, D.O., Loiko, N.G., Gularyan, S.K., *et al.*: Biocrystallization of bacterial nucleoid under stress. *Russian Journal of Physical Chemistry B* 11(5), 833–838 (sep 2017). <https://doi.org/10.1134/s1990793117050128>
35. Szatmári, D., Sárkány, P., Kocsis, B., *et al.*: Intracellular ion concentrations and cation-dependent remodelling of bacterial MreB assemblies. *Scientific Reports* 10(1) (jul 2020). <https://doi.org/10.1038/s41598-020-68960-w>
36. Tereshkin, E.V., Tereshkina, K.B., Kovalenko, V.V., *et al.*: Structure of DPS protein complexes with DNA. *Russian Journal of Physical Chemistry B* 13(5), 769–777 (sep 2019). <https://doi.org/10.1134/s199079311905021x>
37. Tereshkin, E.V., Tereshkina, K.B., Krupyanskii, Y.F.: Molecular dynamics of DNA-binding protein and its 2D-crystals. *Journal of Physics: Conference Series* 2056(1), 012016 (oct 2021). <https://doi.org/10.1088/1742-6596/2056/1/012016>
38. Tereshkin, E., Tereshkina, K., Loiko, N., *et al.*: Interaction of deoxyribonucleic acid with deoxyribonucleic acid-binding protein from starved cells: cluster formation and crystal growing as a model of initial stages of nucleoid biocrystallization. *Journal of Biomolecular Structure and Dynamics* 37(10), 2600–2607 (nov 2018). <https://doi.org/10.1080/07391102.2018.1492458>
39. Tkachenko, A.G.: Stress responses of bacterial cells as mechanism of development of antibiotic tolerance (review). *Applied Biochemistry and Microbiology* 54(2), 108–127 (mar 2018). <https://doi.org/10.1134/s0003683818020114>
40. Uusitalo, J.J., Ingólfsson, H.I., Akhshi, P., *et al.*: Martini coarse-grained force field: Extension to DNA. *Journal of chemical theory and computation* 11(8), 3932–3945 (2015). <https://doi.org/10.1021/acs.jctc.5b00286>
41. Verma, S.C., Qian, Z., Adhya, S.L.: Architecture of the escherichia coli nucleoid. *PLOS Genetics* 15(12), e1008456 (dec 2019). <https://doi.org/10.1371/journal.pgen.1008456>
42. Wolf, S.G., Frenkiel, D., Arad, T., *et al.*: DNA protection by stress-induced biocrystallization. *Nature* 400(6739), 83–85 (jul 1999). <https://doi.org/10.1038/21918>